JACS
JOURNAL OF THE AMERICAN CHEMICAL SOCIETY
pubs.acs.org/JACS
Article

Stereospecific Epitaxial Growth of Bilayered Porous Molecular Networks

Yuan Fang, Benjamin D. Lindner, Iris Destoop, Takashi Tsuji, Zhenzhe Zhang, Rustam Z. Khaliullin, Dmitrii F. Perepichka, Kazukuni Tahara, Steven De Feyter,* and Yoshito Tobe*

Cite This: J. Am. Chem. Soc. 2020, 142, 8662−8671
Read Online

ABSTRACT: Stereocontrolled multilayer growth of supramolecular porous networks at the interface between graphite and a solution was investigated. For this study, we designed a chiral dehydrobenzo[12]annulene (DBA) building block bearing alkoxy chains substituted at the 2 position with hydroxy groups, which enable van der Waals stabilization in a layer and potential hydrogen-bonding interactions between the layers. Bias voltage-dependent scanning tunneling microscopy (STM) experiments revealed the diastereospecificity of the bilayer with respect to both the intrinsic chirality of the building blocks and the supramolecular chirality of the self-assembled networks. Top and bottom layers within the same crystalline domain were composed of the same enantiomers but displayed opposite supramolecular chiralities.

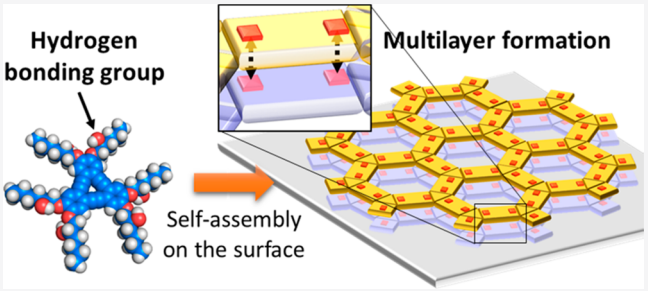

INTRODUCTION

Self-assembled molecular networks (SAMNs) may spontaneously form on surfaces. In contrast to self-assembled monolayers (SAMs) of alkanethiols chemisorbed on gold as an example, organization of the molecules in SAMNs only involves noncovalent interactions. The molecules are physisorbed on the surface, very often lying flat on the surface and giving rise to single-crystalline domains of a few atoms thick that can extend over several square micrometers.[1] Control over the structure and functionality of SAMNs on surfaces or at liquid/solid interfaces has attracted broad interest in the context of nanoscience and nanotechnology.[2,3] Among the various types of two-dimensional (2D) architectures constructed using molecular self-assembly, nanoporous networks are challenging structures because of the necessity to surmount the inherent tendency of molecules to avoid formation of porous structures and assemble in a densely packed geometry. However, they are highly attractive for applications in surface templating, nanopatterning, heterogeneous catalysis, and separations.[4−6] Another challenge in this field is the controlled epitaxial growth of SAMNs orthogonal to the substrate, a process with strong relevance to anchoring three-dimensional (3D) metal−organic materials on surfaces (SURMOFs),[7−9] electronics of semiconducting molecules,[10] and crystal engineering.[11] In particular, stereochemical information about the first few molecular layers can provide insight into the evolution of crystallization from 2D to 3D systems.[12]

Among the various techniques used to probe the structure of ultrathin films, scanning tunneling microscopy (STM) takes a unique position as it provides submolecular resolution, even at the interface between a solid substrate and a solution. Bilayers and multilayers were studied using STM for planar π-conjugated molecules that self-assemble via $\pi-\pi$ interactions[13−22] and for highly polarized molecules undergoing dipole−dipole interactions.[22,23] Typically, the self-assembled second layer does not have a specific registry to the bottom layer. Specific point-to-point interlayer interactions are desirable to precisely control the interlayer geometry.

A few studies on the stereochemical relationship in both the lateral (parallel to the surface) and the longitudinal directions (along the surface normal) of densely packed double layers grown through van der Waals interactions have been performed using chiral molecules with a twisted or helical backbone, such as rubrene,[24] [5]helicene,[25] and [7]-helicene,[26,27] under ultrahigh-vacuum (UHV) conditions. Because of their nonplanar structures, these molecules are packed via van der Waals contacts in a point-to-point manner in both the lateral and the longitudinal directions. They form either a racemate or conglomerate double layer.[28] More specifically, the overlying second layer has opposite or the same handedness with respect to the intrinsic chirality of the molecules themselves and supramolecular chirality of molecular self-assembly. One study reports the nonlinear chiral

Received: January 5, 2020
Published: April 18, 2020

https://dx.doi.org/10.1021/jacs.0c00108
J. Am. Chem. Soc. 2020, 142, 8662−8671

Scheme 1[a]

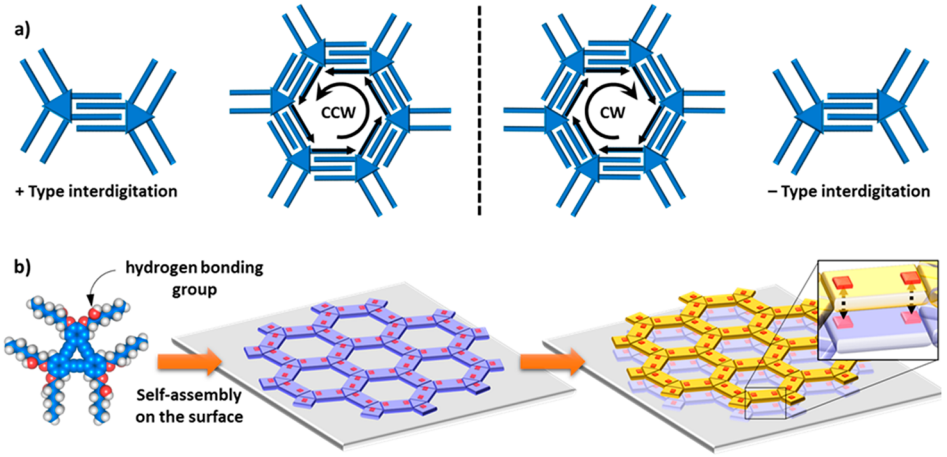

[a](a) Typical supramolecular pores formed by alkylated DBA molecules. The type of alkyl chain interdigitation determines the handedness of the supramolecular pores and the supramolecular networks. (b) Schematic of a self-assembled porous double-layer structure; chirality is ignored for simplicity. In the first step, the DBA molecules bearing polar hydroxy groups (red squares) self-assemble into a honeycomb network on the surface through van der Waals interactions between the alkoxy chains. Growth of the second layer is directed by the van der Waals interactions between the two layers, and possibly with the involvement of longitudinal hydrogen bonding of the hydroxy groups.

amplification effect on bilayers of near-racemic mixtures involving the biased adsorption and organization of the major enantiomer at the liquid/solid interface.[29]

For multilayered porous networks, although a few examples constructed through longitudinal van der Waals or dipole interactions of intrinsically porous macrocyclic molecules have been reported,[30−35] the geometry of their nonbottom layers is not strictly controlled or not determined. To the best of our knowledge, only two reports have described the formation of *porous* double-layer SAMNs using small nonmacrocyclic molecules, but they do not address chirality.[36,37]

Here, we propose an approach to construct self-assembled porous multilayer films with precise control over the interlayer geometry. For this purpose, we selected alkoxy-substituted dehydrobenzo[12]annulene (DBA) derivatives because of their demonstrated ability to form chiral porous honeycomb patterns via the interdigitation of alkoxy chains (Scheme 1)[38,39] and tunability of pore size by varying the alkoxy chain length.[40] We reported the formation of supramolecular networks of a well-defined handedness using chiral DBA (cDBA) molecules, such as **cDBA-OC12**(*S*) and **cDBA-OC12**(*R*) (Chart 1), with methyl-substituted stereogenic centers and their roles in inducing and inversing the supramolecular chirality of networks of achiral DBA molecules.[41−43] On the basis of these results, we hypothesized that replacing the methyl groups with hydrogen-bonding groups would also lead to formation of similar porous chiral networks and furthermore would enforce formation of porous multilayers (Scheme 1), even in a stereocontrolled manner.

Therefore, we designed the chiral DBA derivatives **cDBA-OC6-OH**(*S*) and **cDBA-OC6-OH**(*R*) with a hydroxy group at the 2 position of each hexyloxy chain (Chart 1). We selected hexyloxy chains to promote formation of the porous supramolecular structure with relatively small pores of approximately 1.7 nm in diameter, as revealed previously for **DBA-OC6** (Scheme 1).[44] Upon adsorption and self-assembly on the surface, the homochiral **cDBA-OC6-OH**(*S*) and **cDBA-OC6-OH**(*R*) compounds are expected to form homochiral porous patterns in either the clockwise (CW) or the counterclockwise (CCW) direction through (−) and (+) interdigitation modes of the alkoxy groups, respectively (Scheme 1 and Figure 1), similar to the chiral DBAs with stereogenic methyl groups.[41] More importantly, the hydroxy substituents of **cDBA-OC6-OH**s should orient away from or toward the substrate in an alternating manner, thereby promoting formation of hydrogen bonds and a multilayer structure. Therefore, growth of the overlying layers may occur in a stereospecific manner with respect to the first layer. The stereoselectivity at each step of self-assembly is summarized in Scheme 2 to illustrate the stereochemical outcomes of the formation of the anticipated multilayer structure.

Indeed, we revealed formation of a bilayer of **cDBA-OC6-OH**(*S*) and **cDBA-OC6-OH**(*R*) at the interface between graphite and a liquid using bias voltage-dependent STM observations. The enantiomorphism of the bottom layer was identical to chiral DBAs bearing methyl groups on the chiral center (Steps 1 and 2 in Scheme 2). Most interestingly, multilayer growth occurred in a diastereospecific manner between the top and the bottom layers with respect to both the intrinsic chirality of chiral DBAs, i.e., *S* on *S* vs *S* on *R* (Step 3), and the supramolecular chirality of the molecular network structures, i.e., CW on CW vs CCW on CW (Step 4).

Chart 1. Chemical Structures of cDBA-OC12(*S*), cDBA-OC12(*R*), cDBA-OC6-OH(*S*), cDBA-OC6-OH(*R*), and DBA-OC6

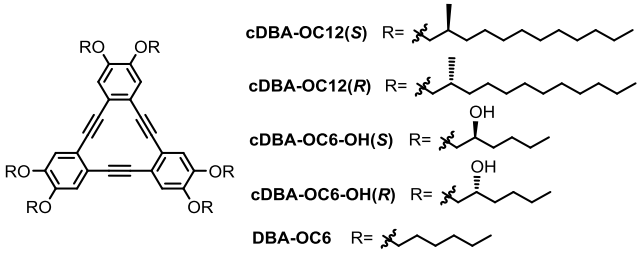

https://dx.doi.org/10.1021/jacs.0c00108
J. Am. Chem. Soc. 2020, 142, 8662−8671

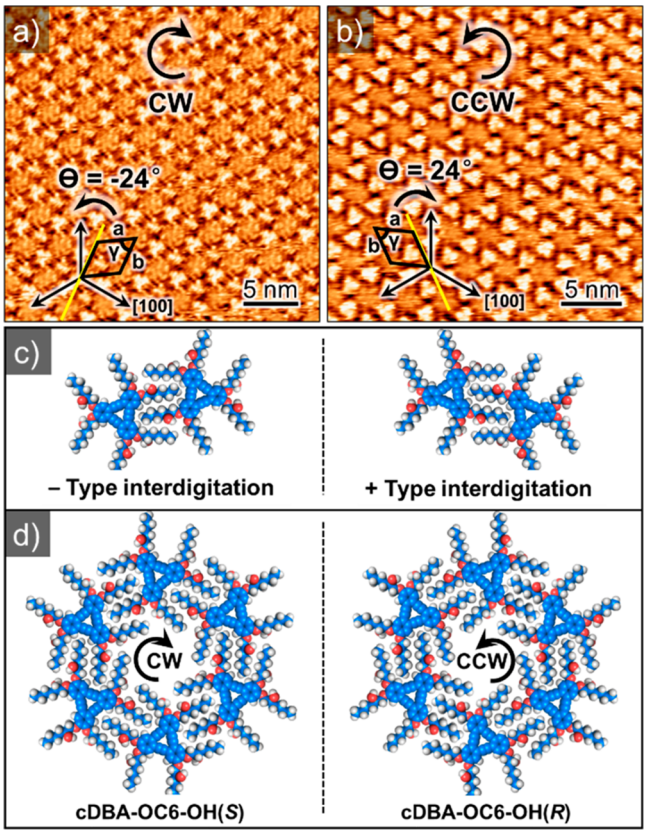

Figure 1. (a and b) STM images of **cDBA-OC6-OH**(*S*) (a) and **cDBA-OC6-OH**(*R*) (b) monolayers formed at the TCB/HOPG interface (2.3×10^{-6} M). Black arrows indicate the graphite reference axes. θ is the angle between a reference axis and one of the unit cell vectors. (c and d) Molecular models of (−) and (+) interdigitation patterns (c) and corresponding CW and CCW nanowells (d) for **cDBA-OC6-OH**(*S*) and **cDBA-OC6-OH**(*R*), respectively. Imaging conditions: (a) I_{set} = 0.2 nA and V_{bias} = −0.2 V and (b) I_{set} = 0.2 nA and V_{bias} = −0.5 V.

RESULTS AND DISCUSSION

Synthesis of cDBA-OC6-OH(*S*) and cDBA-OC6-OH(*R*). Synthesis of the homochiral DBA derivatives **cDBA-OC6-OH**(*S*) and **cDBA-OC6-OH**(*R*) is outlined in Scheme 3 for the *S* enantiomer. We prepared both enantiomers of methoxymethyl (MOM) ethers of 1-bromo-2-hexanol through selective hydrolytic kinetic resolution of chiral epoxides using a chiral (salen)cobalt(III) catalyst,[48] followed by regioselective ring opening of the chiral epoxide and MOM protection to insert the hydroxy-containing chiral alkoxy groups into the DBA core. The chiral alkoxy group was introduced to the iodoalkyne building block by coupling the bromide with 3,4-diiodocatechole, followed by monoalkynylation. Copper-catalyzed cyclotrimerization of the iodoalkyne and subsequent deprotection afforded **cDBA-OC6-OH**(*S*). Using the same procedure, **cDBA-OC6-OH**(*R*) was prepared from the enantiomeric epoxide. The experimental details are described in section 3 of the Supporting Information. Self-assembly of the analytically pure chiral **cDBA-OC6-OH**(*S*) and **cDBA-OC6-OH**(*R*) was analyzed using STM at the interface between highly oriented pyrolytic graphite (HOPG) and one main solvent at various solute concentrations.

Effects of the Solvent and Concentration on the Formation of a Monolayer and Multilayers. In the first step, we investigated the self-assembly of relatively low concentrations of homochiral enantiomers and racemates of **cDBA-OC6-OH**(*S*) and **cDBA-OC6-OH**(*R*) at liquid/solid interfaces. Regardless of the solvent [1,2,4-trichlorobenzene (TCB, Figure 1), 1-octanol (Figure S1a), or 1-phenyloctane (Figure S1b)],[49] each enantiomer self-assembles into the typical nanoporous honeycomb networks with opposite 2D chirality, similar to chiral DBAs with stereogenic methyl groups, such as **cDBA-OC12**(*S*) and **cDBA-OC12**(*R*) (Chart 1).[41] The DBA cores are lying flat on the substrate, and the molecules are linked by van der Waals interactions between the interdigitated alkoxy chains. Figure 1 displays STM images of **cDBA-OC6-OH**(*S*) and **cDBA-OC6-OH**(*R*) at the TCB/HOPG interface, together with a simplified molecular model. The unit cell parameters are $a = b = 3.2$ nm, and the angle $\gamma = 60°$. These unit cell parameters are identical to the achiral analogue **DBA-OC6** without hydroxy groups.[44] In most STM images, although the alkoxy chains are not clearly visible, the type of interdigitation (+ or −) and the supramolecular chirality [clockwise (CW) or counterclockwise (CCW)] can be determined from the lateral shift of adjacent DBA cores (Figure 1a–d). The overall handedness of the network can also be determined by the signs of the rotation angles of a unit cell vector with respect to one of the symmetry axes of graphite (Figures 1a, 1b, and S2).

Consistent with the stereogenic methyl substitution on the alkyl chains of **cDBA-OC12**(*S*) and **cDBA-OC12**(*R*),[41,42] these compounds show enantiomorphous pattern formation. The *S* enantiomer exclusively produces CW nanowells via (−)-type interdigitation, while the *R* enantiomer produces (+) interdigitated pairs, leading to formation of CCW nanowells (Figure 1). Because the supramolecular chirality of the network is the same as **cDBA-OC12**(*S*) and **cDBA-OC12**(*R*),[41,42] the roles of the hydroxy and methyl groups are likely similar in biasing the alkoxy chain interdigitation type and establishing the chirality of the nanowell domains (Step 1 of Scheme 2). The observed selectivity is consistent with molecular mechanics simulations under periodic boundary conditions (PBC) on a bilayered graphene whose geometry was fixed using the COMPASS force field. For the *R* enantiomer, the CCW nanowell formed by the (+) interdigitation type is 1.0 kcal mol^{-1} more stable than the CW nanowell with the (−) interdigitation type (Figure S3).

Once again, similar to their chiral analogues containing stereogenic methyl groups,[41,42] when a racemic mixture of **cDBA-OC6-OH**(*S*) and **cDBA-OC6-OH**(*R*) was deposited at the liquid/solid interface, enantiomorphous domains formed with equal surface coverage. As an example, Figure 2 displays an STM image of racemic **cDBA-OC6-OH** at the TCB/HOPG interface. Therefore, we conclude that a racemic conglomerate is formed at the liquid/solid interface; both enantiomers assemble in different domains and are phase separated (Step 2 of Scheme 2).

In contrast to any known DBAs, increasing the concentration of **cDBA-OC6-OH** leads to noticeable changes in the structure and contrast of the STM images, except when 1-octanol is used as the solvent (Figure S4). Carefully increasing the concentration from 2.3×10^{-6} to 2.5×10^{-6} M in TCB[49] produces two different types of contrast for the triangular DBA core (Figures 3a and S5). In the higher magnification images (Figure 3b–d), the brighter cDBA molecules are indicated by green dotted triangles. The cDBAs with the same relative position as the brighter cDBA molecules are indicated by solid

https://dx.doi.org/10.1021/jacs.0c00108
J. Am. Chem. Soc. 2020, 142, 8662−8671

Scheme 2. Schematic of the Stereoselectivity in the Formation of a Self-Assembled Bilayer of Chiral DBA Molecules[a]

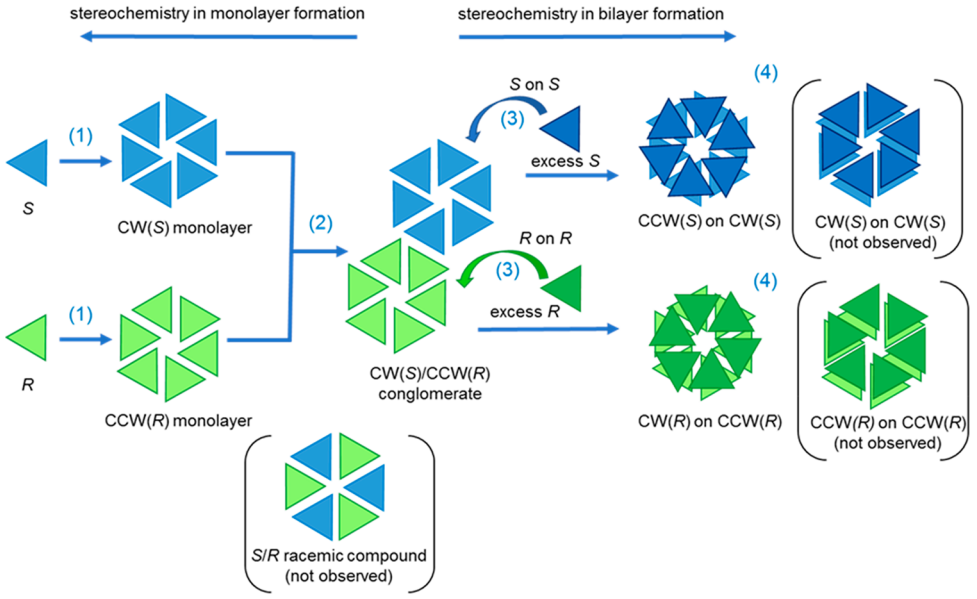

[a]Blue and green triangles represent **cDBA-OC6-OH**(*S*) and **cDBA-OC6-OH**(*R*), respectively. Chirality arising from the relationship between the orientation of the molecules (or unit cell) with respect to the substrate symmetry axes is not considered.[45−47] Step 1: Supramolecular enantiospecific self-assembly of **cDBA-OC6-OH**(*S*) and **cDBA-OC6-OH**(*R*) forming clockwise (CW) and counterclockwise (CCW) patterns, respectively (see also Figure 1d). Step 2: Stereoselectivity in a 1:1 mixture of **cDBA-OC6-OH**(*S*) and **cDBA-OC6-OH**(*R*) forming a domain-separated "conglomerate" consisting of CW and CCW domains; corresponding "racemic compound" was not observed. Step 3: Diastereospecificity in bilayer formation with respect to the intrinsic chirality of cDBAs in the presence of excess **cDBA-OC6-OH**(*S*) or **cDBA-OC6-OH**(*R*). Formation of a bilayer with the same handedness, i.e., **cDBA-OC6-OH**(*S*) on top of **cDBA-OC6-OH**(*S*) or **cDBA-OC6-OH**(*R*) on top of **cDBA-OC6-OH**(*R*), is favored. Step 4: Diastereospecificity in bilayer formation with respect to the supramolecular chirality; bilayers consisting of antipodal (CW/CCW) patterns of the honeycomb structure are favored over patterns with the same handedness (CW/CW or CCW/CCW).

Scheme 3. Outline of the Synthesis of cDBA-OC6-OH(*S*)[a]

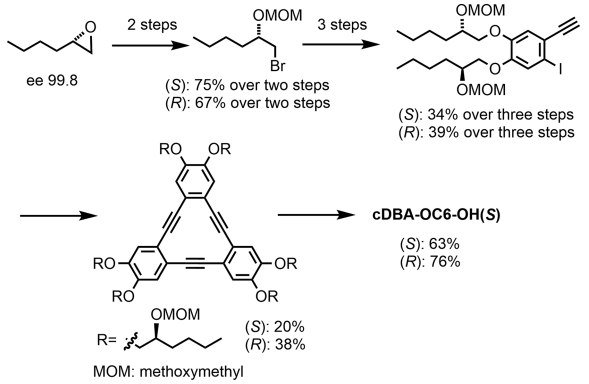

[a]**cDBA-OC6-OH**(*R*) was prepared using the same procedure starting from the enantiomeric epoxide.

green triangles, while others are indicated by solid black triangles. From these high-resolution data, the brighter triangle cores of molecules numbered 1, 2, and 3 appear to be rotated by 0°, 51°, and 35° with respect to other reference solid green triangles (Figures 3b−d and S5e−g). A line profile (Figure 3e, S5a, S5c, and S5d) shows that the "high" DBA molecules are almost twice as high as the "low" DBA molecules. On the basis of the height of these nonperiodic protrusions and their varying orientations, we conclude that increasing the concentration led to the adsorption of single molecules in the second layer.

A further increase in the concentration to 2.6×10^{-6} M increases the density of molecules in the second layer (Figure

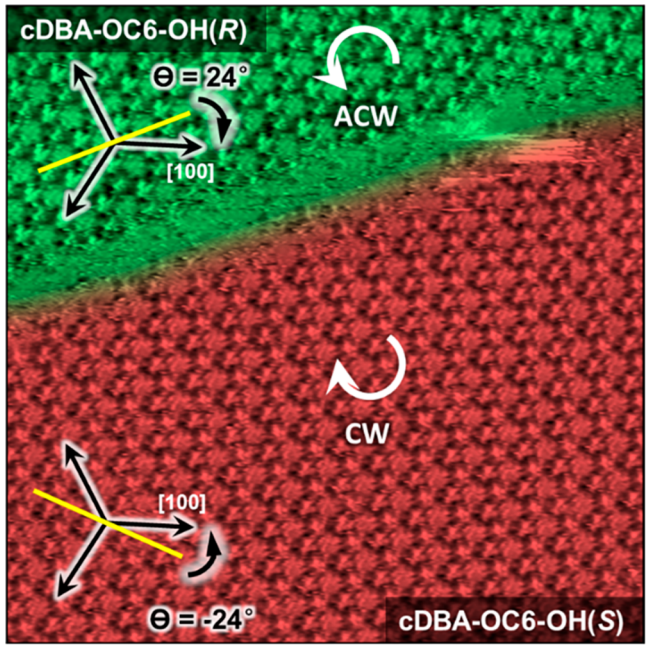

Figure 2. STM image showing the enantiomorphous domains of racemic chiral **cDBA-OC6-OH** at the TCB/HOPG interface ($C = 5.0 \times 10^{-6}$ M, image size 50 × 50 nm^2). (Top left and bottom right) **cDBA-OC6-OH**(*R*) and **cDBA-OC6-OH**(*S*) domains are colored green and red, respectively. HOPG main symmetry axes are indicated by black arrows. **cDBA-OC6-OH**(*S*) and **cDBA-OC6-OH**(*R*) domains are rotated by 24° and −24° with respect to the surface reference directions (Figure S2). Imaging conditions: I_{set} = 0.2 nA and V_{bias} = −0.2 V.

https://dx.doi.org/10.1021/jacs.0c00108
J. Am. Chem. Soc. 2020, 142, 8662−8671

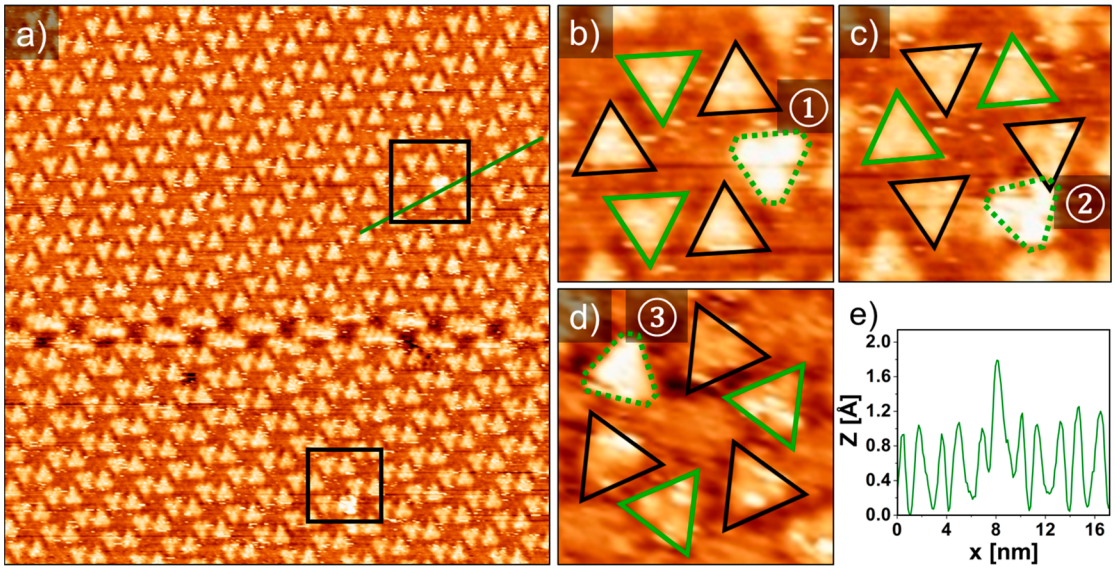

Figure 3. High-resolution STM image of **cDBA-OC6-OH**(*S*) in TCB ($C = 2.5 \times 10^{-6}$ M) reveals isolated molecules on top of the bottom layer. (a) Large-scale image (53×53 nm^2). (b and c) Digital magnification of the image shown in a. Full-scale image of d is presented in Figure S5b. (b–d) Green dotted triangles indicate the orientation of the bright DBAs. cDBAs with the same relative position as the brighter cDBAs are indicated by solid green triangles, while others are indicated by solid black triangles. (e) Line profile across a "high" DBA molecule, as indicated by the green line in a. (a–d) Imaging conditions: I_{set} = 0.2 nA and V_{bias} = −1.4 V.

4), with formation of on-top dimers. Interestingly, the relative orientation of the triangles in this on-top dimer (Figure 4b and

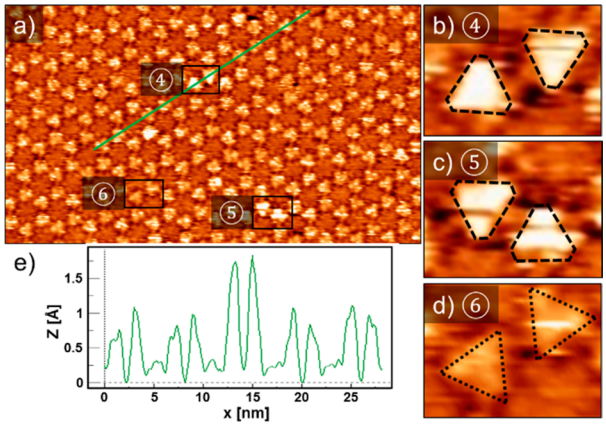

Figure 4. High-resolution STM image of **cDBA-OC6-OH**(*S*) in TCB reveals the initial formation of second-layer dimers. (a) Large-scale image (42×24 nm^2; $C = 2.6 \times 10^{-6}$ M). (b–d) Digital magnification of the image shown in a. Triangle cores of the second layer dimer (b and c) appear to face each other as opposed to being shifted for monolayer dimers (d). Imaging condition: I_{set} = 0.2 nA and V_{bias} = −1.4 V. (e) Line profile across a second layer dimer, as indicated by the green line in a.

4c) differs from the relative orientation of adjacent molecules one layer below ((−)-type interdigitation, Figure 4d). In the former case, maximum overlap is observed between the two adjacent sides of neighboring triangles, as opposed to the apparent shift of the molecules in the layer underneath.

A further increase in the concentration (2.7×10^{-6} M) also leads to formation of a more extended second layer (Figure S6a). Actually, the second layer appears to be adsorbed so strongly to the first layer that it is unable to easily be removed by rinses with the solvent (Figure S6b). This finding differs from the SAMN formed from **DBA-OC6**, which does not show any multilayer growth, even at a very high solution concentration of 1.2×10^{-2} M (Figure S7). For related compounds carrying a methyl group on the chiral center, **cDBA-OC12**(*S*) and **cDBA-OC12**(*R*), multilayer formation was never observed in the same solvents.[41]

A partial double layer was also observed in a 1-phenyloctane solution for **cDBA-OC6-OH** (Figure S8), while regardless of the concentration, only monolayer formation was observed in 1-octanol (Figure S4). These results support but do not validate our hypothesis that longitudinal hydrogen bonding promotes growth of a second layer.

Bias Voltage Dependence of Monolayer versus Multilayers Imaging. At a high concentration of the chiral DBA (>2.9×10^{-6} M) in TCB, the image contrast depends on the imaging conditions. For example, the two sequential images (taken 2 min apart) in Figure 5a and 5b for **cDBA-OC6-OH**(*R*) (1×10^{-3} M) at the TCB/HOPG interface clearly display the effect of the bias voltage. Figure 5a was recorded at the bias voltage (V_{bias}) of −0.5 V, whereas Figure 5b was recorded at V_{bias} of −1.2 V. The SAMN in Figure 5a contains narrow domain boundaries, as indicated by white dashed lines, which are typically less than one molecule wide. The STM image recorded at −1.2 V (Figure 5b) displays a remarkable difference in contrast, showing some dark trenches that appear to coincide with the white lines in Figure 5a to some extent. We tentatively interpret the difference in contrast at the more negative sample bias to visualization of the top layer of a multilayer structure. Additional higher magnification images in Figure 5c with the respective height profiles (Figure 5d) at large negative sample bias (V_{bias} = −1.1 V) further support formation of double layers. The line profile (Figure 5d) shows a significant difference in height between the low and high DBA molecules, which supports the interpretation that the high molecules are part of the top of a double layer or multilayer. Figure 5c reveals details of the "dark trenches": the multilayers do not readily grow at the domain boundaries.

https://dx.doi.org/10.1021/jacs.0c00108
J. Am. Chem. Soc. 2020, 142, 8662−8671

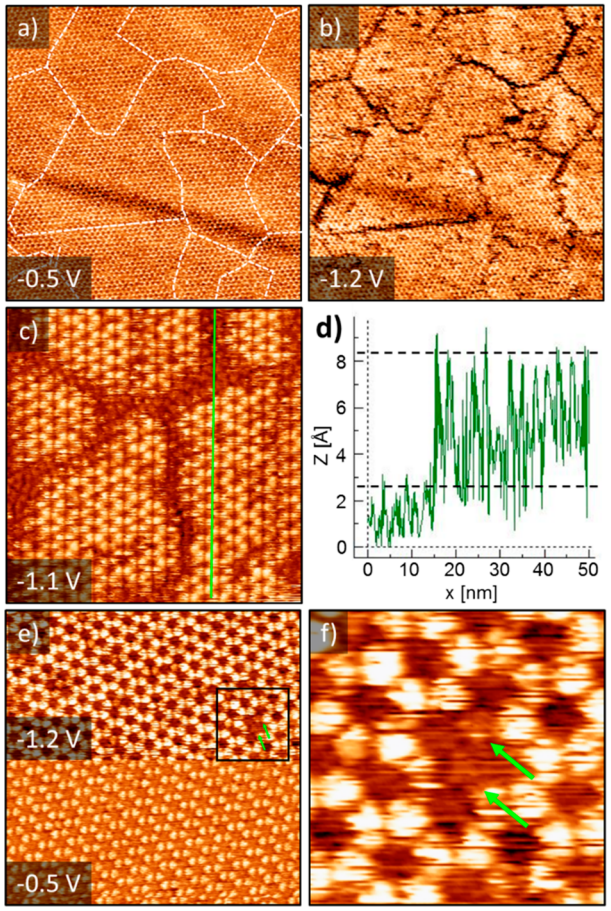

Figure 5. STM image of **cDBA-OC6-OH**(*S*) in TCB (1×10^{-3} M) showing the effect of the bias voltage on the contrast of the multilayer structure. (a and b) Sequential STM images (170×170 nm^2) captured at a bias voltage of −0.5 (a, showing monolayer) and −1.2 V (b, showing double layer with dark trenches), respectively. White dashed lines in (a) indicate domain borders. (c) Higher magnification image (55×55 nm^2) showing more details of the dark trenches captured at a sample bias voltage of −1.1 V. (d) Line profiles along the green lines indicated in c. (e) In the middle of the image, the voltage increased from −1.2 (showing double layer) to −0.5 V (showing monolayer) (50×50 nm^2) from top to bottom. In the top half of the image, defects in the top layer (marked by green arrows in e and its higher magnification image in f) allow us to visualize molecules in the lower layer, which appear darker than the surrounding molecules. For all images, I_{set} = 0.2 nA.

By switching the bias voltage during scanning, the imaging mode is able to be switched reversibly between multiple and single layers (Figure 5e). During scanning, the voltage was increased from −1.2 to −0.5 V. As a result, the top half of the image appears brighter than the bottom half, consistent with the imaging of a multilayer at larger negative sample bias and of a monolayer at smaller negative bias. Similar bias−voltage dependences of monolayer and multilayers have been reported for some other systems.[16,20,37,50] Upon decreasing the absolute value of the voltage, the tip−substrate distance decreases and the STM tip likely penetrates through the double layer to image the bottom layer (see the SI, including Figure S12, for more information).

Stereospecificity in Bilayer Formation. At low concentrations, racemic solutions of **cDBA-OC6-OH** (total concentrations of 5×10^{-6} M for TCB (Figure 2) and 2×10^{-5} M for 1-phenyloctane (Figure S9)) self-assemble into a domain-separated conglomerate consisting of domains of each enantiomer. Similarly, a racemate at high concentration (>1×10^{-4} M) also tends to form a domain-separated bilayer (Figure S10). We investigated if bilayer formation is diastereospecific in terms of (i) the intrinsic chirality of cDBAs in the first and second layers (Step 3 in Scheme 2) and (ii) supramolecular chirality, i.e., CW/CCW patterns of the honeycomb structure, of the first and second layers (Step 4 in Scheme 2).

First, we prepared a low-concentration, equimolar solution of both enantiomers in TCB and placed 20 μL of this solution in a liquid cell with the HOPG substrate. After network formation was verified using STM, an excess amount of one of the enantiomers, **cDBA-OC6-OH**(*R*) in the case of Figure 6,

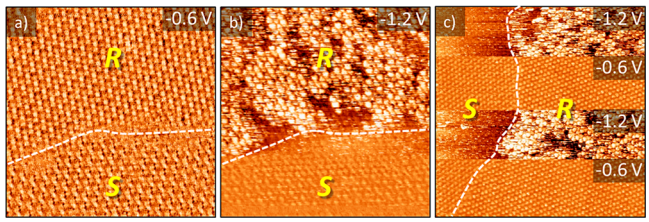

Figure 6. Enantioselective formation of a multilayer structure. Sequential addition of a 1:1 mixture of **cDBA-OC6-OH**(*S*) and **cDBA-OC6-OH**(*R*) (concentration of each enantiomer = 3×10^{-4} M, 20 μL), followed by addition of **cDBA-OC6-OH**(*R*) (1.2×10^{-3} M, 20 μL) in a liquid cell at the TCB/HOPG interface. (a−c) Images were captured after excess **cDBA-OC6-OH**(*R*) was added. White dashed lines indicate domain boundaries. (a and b) Sequential images captured at the same location. (a) Image of the bottom layer at −0.6 V. Top domain is determined to be **cDBA-OC6-OH**(*R*), and bottom domain is determined to be **cDBA-OC6-OH**(*S*). For more details, see Figure S11. (b) At −1.2 V, double-layer formation was observed only on top of the **cDBA-OC6-OH**(*R*) domain. (c) STM image obtained by modulating the bias voltage during the scanning process. (a−c) Image size 100×100 nm^2. I_{set} = 0.2 nA, and V_{bias} is indicated in the images.

was added to the liquid cell. This sequential addition protocol ensures that the domains of both enantiomers initially formed. STM imaging at a small negative bias of −0.6 V clearly revealed formation of separate CW and CCW domains in the first layer (Figure 6a), similar to STM images of monolayers formed at a low concentration (Figure 2). The domains in the upper and lower half of Figure 6a are attributed to **cDBA-OC6-OH**(*R*) and **cDBA-OC6-OH**(*S*) domains, respectively, based on the signs of the domain rotation angles with respect to one of the symmetry axes of graphite (Figures 2 and S11). By decreasing the bias voltage from −0.6 to −1.2 V, a second layer is observed *exclusively* on top of the CCW domain of **cDBA-OC6-OH**(*R*) (Figure 6b). Given the excess amount of **cDBA-OC6-OH**(*R*) in solution, the exclusive observation of the double layer on a CCW domain indicates that the top layer also consists of **cDBA-OC6-OH**(*R*). Experiments in which an excess of **cDBA-OC6-OH**(*S*) was added produced similar results, as shown in Figure S13. In the latter case, bilayer formation is only observed on CW domains. When using a premixed solution of both enantiomers with an excess of one of the enantiomers, a second layer is only observed on top of the domains formed by the major enantiomer, consistent with the results obtained upon sequential addition (Figure S14).

https://dx.doi.org/10.1021/jacs.0c00108
J. Am. Chem. Soc. 2020, 142, 8662−8671

In addition to the domain-dependent layer growth, we are also able to monitor each layer separately depending on the chosen STM bias voltage. The contrast switch in the image occurs instantaneously as the bias voltage is modulated. In Figure 6c, double-layer formation is observed at −1.2 V, while the underlying bottom layer is revealed at −0.6 V. This approach allows us to determine the handedness of the bottom layer and confirms that in the presence of excess **cDBA-OC6-OH**(*R*), bilayer formation is only observed on top of the CCW bottom layer domains. Figure S13 illustrates this principle for excess **cDBA-OC6-OH**(*S*). When a racemic solution of cDBAs at relatively high concentration was used, domain-separated bilayers consisting of homochiral domains of cDBA were observed, although we did not determine their stereochemistry (Figure S10).

No evidence is found that concentration-dependent aggregation in solution is involved in the formation of these structures. In a $CDCl_3$ solution, cDBAs exhibit a small concentration-dependent ^{1}H NMR chemical shift, suggesting weak aggregation (see Supporting Information section 5). However, this shift is nearly identical in homochiral and racemate solutions, refuting the idea of stereospecific association in solution. The enantioselective formation of the double-layer structure with respect to the intrinsic chirality of cDBA is therefore concluded to be a specific phenomenon occurring at the interface between the solid HOPG support and the solution on top.

Next, we investigated whether bilayer formation is diastereospecific with respect to supramolecular chirality of the first and second layers (Step 4, Scheme 2). For example, for the *S* enantiomer, the first layer adopts the CW honeycomb pattern through the (−)-type interdigitation of the alkoxy chains (Figure 1a). Depending on whether the second layer adopts the antipodal CCW pattern or the same-handed CW pattern, the double layer will be diastereomeric with respect to supramolecular chirality (Step 4 in Scheme 2). Homochiral solutions were used to probe the supramolecular chirality of the second layer while excluding the possibility of interference from the DBA molecules with the opposite chirality. Figure 7a shows an STM image of **cDBA-OC6-OH**(*S*) (1×10^{-3} M) at the TCB/HOPG interface. The triangular features, which are highlighted by the black dotted lines, form a pattern with *p6m* plane group symmetry, as opposed to the chiral *p6* symmetry of the monolayer (Figure 7a, inset).[51] The appearance of this apparent achiral feature is potentially explained in terms of an offset of shifts between overlapping antipodal triangles, as shown in Figure 7b. This type of staggered packing was observed for the crystal packing of other DBA derivatives (achiral), as evidenced by single-crystal structures.[52,53] Accordingly, we deduce that the second layer adopts an antipodal supramolecular chirality, i.e., CCW on CW and CW on CCW, for **cDBA-OC6-OH**(*S*) and **cDBA-OC6-OH**(*R*), respectively.

A series of molecular mechanics (MM) optimizations using the COMPASS force field were performed to obtain insights into the molecular structure of and intermolecular interactions in different bilayers. Table S1 shows the lowest energy local minima we observed for bilayers composed of **cDBA-OC6-OH**(*R*) and **cDBA-OC6-OH**(*R*)/**cDBA-OC6-OH**(*S*) (Figure S15). When both layers have the same supramolecular chirality (e.g., CCW/CCW or Figure S15a), their DBA cores are laterally shifted with respect to each other, and when the layers differ in supramolecular chirality (e.g., CCW/CW or Figure S15c), their DBA cores are rotated with respect to each other. This finding forms the basis for the assignment of chirality of the layers in STM images of different bilayers (Figure S15). The MM optimizations also reveal that certain OH groups are capable of forming hydrogen bonds (OH···O distances ranging between ca. 1.7 and 2.1 Å, Table S2), providing additional stabilization to bilayer structures. The estimated energy values (Table S1) are not consistent with the experimental results. This latter point is not surprising considering the conformational flexibility in these systems and our neglect of the role of the solvent. In addition, kinetic factors may overrule thermodynamic equilibrium. Indeed, annealing of a solution of **cDBA-OC6-OH**(*R*) in TCB on HOPG at 80 °C for 10 min resulted in formation of a new phase, the trimer phase (Figure S16).[38] This result indicates the complexity of the system, where the multilayer is a metastable or a kinetically trapped phase. A further detailed analysis of the stability of the multilayer vs other phases is required to understand the thermodynamics of the present complicated system.

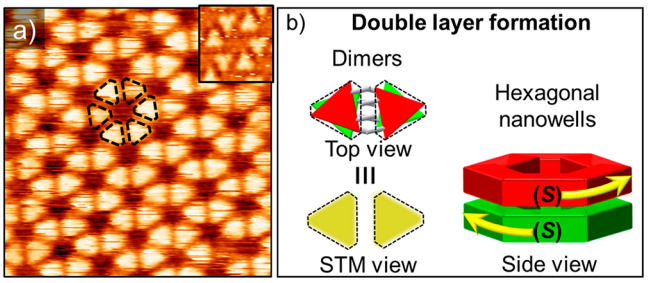

Figure 7. (a) STM image of the self-assembly of a multilayered **cDBA-OC6-OH**(*S*) structure (1×10^{-3} M) at the TCB/HOPG interface (20×20 nm^2). Black dashed triangles indicate the apparent orientations of the triangle DBA cores of the multilayer. (Inset) Monolayer self-assembly of **cDBA-OC6-OH**(*S*). Note the change in the plane group from chiral *p6* to achiral *p6m* for the monolayer (inset) and double layer (a), respectively. (b) Proposed multilayer growth model where the bottom layer and the second layer have opposite interdigitation patterns. At the dimer level for **cDBA-OC6-OH**(*S*), the bottom layer (green) adopts the (−) interdigitation pattern (see Figure 1) while the second layer (red) adopts the (+) interdigitation pattern. At the supramolecular hexagonal nanowell level, the bottom layer (green) exhibits the CW pattern (see Figure 1) while the second layer (red) displays the CCW pattern. Red and green triangle cores are right on top of each other but rotated. STM contrast shows a superimposed image of two rotated DBA triangle cores in the first and second layer, as outlined by the dotted triangles. Imaging conditions: I_{set} = 0.2 nA and V_{bias} = −1.4 V.

CONCLUSIONS

For the first time, we were able to achieve the stereocontrolled growth of a multilayered supramolecular porous network at the liquid/solid interface. DBA derivatives bearing alkoxy chains substituted at the 2 position with a hydroxy group were designed to extend the growth toward the third dimension. Upon forming a self-assembled monolayer, three hydroxy groups are pointing away from the surface and allow for hydrogen-bonding interactions with the overlaying layer. Under appropriate concentration and solvent conditions, double-layer formation was confirmed by bias voltage-dependent STM observations. Both lateral van der Waals interactions and possibly also longitudinal hydrogen bonds contribute to formation of multilayers. On the basis of the experimental evidence, formation of homochiral double layers, i.e., bilayer

https://dx.doi.org/10.1021/jacs.0c00108
J. Am. Chem. Soc. 2020, 142, 8662−8671

formation, is a stereospecific process, and the top and bottom layer have the same intrinsic chirality. Surprisingly, the overlaying layer adopts opposite supramolecular handedness with respect to that of the first layer, highlighting the complexity of self-assembly pathways and the mechanisms involved in the amplification of chirality.

■ ASSOCIATED CONTENT

Supporting Information

The Supporting Information is available free of charge at https://pubs.acs.org/doi/10.1021/jacs.0c00108.

Experimental details, MM simulations, additional STM images, and synthesis of chiral DBA derivatives (PDF)

■ AUTHOR INFORMATION

Corresponding Authors

Steven De Feyter − *Department of Chemistry, Division of Molecular Imaging and Photonics, KU Leuven, Leuven B-3001, Belgium;* orcid.org/0000-0002-0909-9292; Email: steven.defeyter@kuleuven.be

Yoshito Tobe − *Division of Frontier Materials Science, Graduate School of Engineering Science and The Institute of Scientific and Industrial Research, Osaka University, Ibaraki, Osaka 567-0047, Japan; Department of Applied Chemistry, National Chiao Tung University, Hsinchu 30010, Taiwan;* orcid.org/0000-0002-1795-5829; Email: tobe@chem.es.osaka-u.ac.jp

Authors

Yuan Fang − *Department of Chemistry, Division of Molecular Imaging and Photonics, KU Leuven, Leuven B-3001, Belgium; Department of Chemistry, McGill University, Montreal, Québec H3A 0B8, Canada;* orcid.org/0000-0002-4846-1725

Benjamin D. Lindner − *Division of Frontier Materials Science, Graduate School of Engineering Science, Osaka University, Ibaraki, Osaka 567-0047, Japan*

Iris Destoop − *Department of Chemistry, Division of Molecular Imaging and Photonics, KU Leuven, Leuven B-3001, Belgium*

Takashi Tsuji − *Division of Frontier Materials Science, Graduate School of Engineering Science, Osaka University, Ibaraki, Osaka 567-0047, Japan*

Zhenzhe Zhang − *Department of Chemistry, McGill University, Montreal, Québec H3A 0B8, Canada;* orcid.org/0000-0002-9983-7729

Rustam Z. Khaliullin − *Department of Chemistry, McGill University, Montreal, Québec H3A 0B8, Canada;* orcid.org/0000-0002-9073-6753

Dmitrii F. Perepichka − *Department of Chemistry, McGill University, Montreal, Québec H3A 0B8, Canada;* orcid.org/0000-0003-2233-416X

Kazukuni Tahara − *Division of Frontier Materials Science, Graduate School of Engineering Science, Osaka University, Ibaraki, Osaka 567-0047, Japan; Department of Applied Chemistry, School of Science and Technology, Meiji University, Kawasaki 214-8571, Japan;* orcid.org/0000-0002-3634-541X

Complete contact information is available at: https://pubs.acs.org/10.1021/jacs.0c00108

Notes

The authors declare no competing financial interest.

■ ACKNOWLEDGMENTS

This study was supported by JSPS KAKENHI (JP15H02164 and JP18H05353 for Y.T. and JP17K19130 and JP19H04597 for K.T.) and by the Higher Education Sprout Project of the National Chiao Tung University and Ministry of Education (MOE), Taiwan, which are gratefully acknowledged. The authors also acknowledge financial support from the Fund of Scientific Research Flanders (FWO) under grant EOS 30489208 and KU Leuven-Internal Funds. The research leading to these results has also received funding from the European Research Council under the European Union's Seventh Framework Programme (FP7/2007-2013)/ERC Grant Agreement No. 340324 to S.D.F. The work in Canada was supported by NSERC Discovery Grants (to R.K. and to D.F.P.). Y.F. acknowledges NSERC and FQRNT post-doctoral fellowship.

■ REFERENCES

(1) Goronzy, D. P.; Ebrahimi, M.; Rosei, F.; Arramel; Fang, Y.; De Feyter, S.; Tait, S. L.; Wang, C.; Beton, P. H.; Wee, A. T. S.; Weiss, P. S.; Perepichka, D. F. Supramolecular Assemblies on Surfaces: Nanopatterning, Functionality, and Reactivity. *ACS Nano* **2018**, *12*, 7445−7481.

(2) Sosa-Vargas, L.; Kim, E.; Attias, A.-J. Beyond "decorative" 2D supramolecular self-assembly: strategies towards functional surfaces for nanotechnology. *Mater. Horiz.* **2017**, *4*, 570−583.

(3) Mali, K. S.; Pearce, N.; De Feyter, S.; Champness, N. R. Frontiers of supramolecular chemistry at solid surfaces. *Chem. Soc. Rev.* **2017**, *46*, 2520−2542.

(4) Bonifazi, D.; Mohnani, S.; Llanes-Pallas, A. Supramolecular Chemistry at Interfaces: Molecular Recognition on Nanopatterned Porous Surfaces. *Chem. - Eur. J.* **2009**, *15*, 7004−7025.

(5) Ma, X.; Yang, Y.; Deng, K.; Zeng, Q.; Zhao, K.; Wang, C.; Bai, C. Molecular miscibility characteristics of self-assembled 2D molecular architectures. *J. Mater. Chem.* **2008**, *18*, 2074−2081.

(6) Iritani, K.; Tahara, K.; De Feyter, S.; Tobe, Y. Host-Guest Chemistry in Integrated Porous Space Formed by Molecular Self-Assembly at Liquid-Solid Interfaces. *Langmuir* **2017**, *33*, 4601−4618.

(7) Stepanow, S.; Lingenfelder, M.; Dmitriev, A.; Spillmann, H.; Delvigne, E.; Lin, N.; Deng, X.; Cai, C.; Barth, J. V.; Kern, K. Steering molecular organization and host-guest interactions using two-dimensional nanoporous coordination systems. *Nat. Mater.* **2004**, *3*, 229−233.

(8) Heinke, L.; Gu, Z.; Woell, C. The surface barrier phenomenon at the loading of metal-organic frameworks. *Nat. Commun.* **2014**, *5*, 4562.

(9) Liu, J.; Zhou, W.; Liu, J.; Howard, I.; Kilibarda, G.; Schlabach, S.; Coupry, D.; Addicoat, M.; Yoneda, S.; Tsutsui, Y.; Sakurai, T.; Seki, S.; Wang, Z.; Lindemann, P.; Redel, E.; Heine, T.; Wöll, C. Photoinduced Charge-Carrier Generation in Epitaxial MOF Thin Films: High Efficiency as a Result of an Indirect Electronic Band Gap? *Angew. Chem., Int. Ed.* **2015**, *54*, 7441−7445.

(10) Ciesielski, A.; Samori, P. Supramolecular Approaches to Graphene: From Self-Assembly to Molecule-Assisted Liquid-Phase Exfoliation. *Adv. Mater.* **2016**, *28*, 6030−6051.

(11) Zheng, Q. N.; Liu, X. H.; Chen, T.; Yan, H. J.; Cook, T.; Wang, D.; Stang, P. J.; Wan, L. J. Formation of Halogen Bond-Based 2D Supramolecular Assemblies by Electric Manipulation. *J. Am. Chem. Soc.* **2015**, *137*, 6128−6131.

(12) Dutta, S.; Gellman, A. J. Enantiomer surface chemistry: conglomerate versus racemate formation on surfaces. *Chem. Soc. Rev.* **2017**, *46*, 7787−7839.

(13) Samori, P.; Severin, N.; Simpson, C. D.; Mullen, K.; Rabe, J. P. Epitaxial composite layers of electron donors and acceptors from very large polycyclic aromatic hydrocarbons. *J. Am. Chem. Soc.* **2002**, *124*, 9454−9457.

(14) Samorí, P.; Fechtenkötter, A.; Jäckel, F.; Böhme, T.; Müllen, K.; Rabe, J. P. Supramolecular Staircase via Self-Assembly of Disklike Molecules at the Solid-Liquid Interface. *J. Am. Chem. Soc.* **2001**, *123*, 11462−11467.
(15) Dossel, L. F.; Kamm, V.; Howard, I. A.; Laquai, F.; Pisula, W.; Feng, X.; Li, C.; Takase, M.; Kudernac, T.; De Feyter, S.; Mullen, K. Synthesis and controlled self-assembly of covalently linked hexa-peri-hexabenzocoronene/perylene diimide dyads as models to study fundamental energy and electron transfer processes. *J. Am. Chem. Soc.* **2012**, *134*, 5876−5886.
(16) Piot, L.; Marie, C.; Feng, X.; Muellen, K.; Fichou, D. Hierarchical Self-Assembly of Edge-On Nanocolumnar Superstructures of Large Disc-Like Molecules. *Adv. Mater.* **2008**, *20*, 3854−3858.
(17) Huang, Y. L.; Chen, W.; Wee, A. T. S. Molecular Trapping on Two-Dimensional Binary Supramolecular Networks. *J. Am. Chem. Soc.* **2011**, *133*, 820−825.
(18) Yoshimoto, S.; Tsutsumi, E.; Suto, K.; Honda, Y.; Itaya, K. Molecular assemblies and redox reactions of zinc(II) tetraphenylporphyrin and zinc(II) phthalocyanine on Au(111) single crystal surface at electrochemical interface. *Chem. Phys.* **2005**, *319*, 147−158.
(19) Uemura, S.; Sakata, M.; Taniguchi, I.; Hirayama, C.; Kunitake, M. In situ observation of coronene epitaxial adlayers on Au(111) surfaces prepared by the transfer of Langmuir films. *Thin Solid Films* **2002**, *409*, 206−210.
(20) Ivasenko, O.; MacLeod, J. M.; Chernichenko, K. Y.; Balenkova, E. S.; Shpanchenko, R. V.; Nenajdenko, V. G.; Rosei, F.; Perepichka, D. F. Supramolecular assembly of heterocirculenes in 2D and 3D. *Chem. Commun.* **2009**, 1192−1194.
(21) Ikeda, T.; Asakawa, M.; Goto, M.; Miyake, K.; Ishida, T.; Shimizu, T. STM Observation of Alkyl-Chain-Assisted Self-Assembled Monolayers of Pyridine-Coordinated Porphyrin Rhodium Chlorides. *Langmuir* **2004**, *20*, 5454−5459.
(22) Skomski, D.; Jo, J.; Tempas, C. D.; Kim, S.; Lee, D.; Tait, S. L. High-Fidelity Self-Assembly of Crystalline and Parallel-Oriented Organic Thin Films by $\pi-\pi$ Stacking from a Metal Surface. *Langmuir* **2014**, *30*, 10050−10056.
(23) Niederhausen, J.; Kersell, H. R.; Christodoulou, C.; Heimel, G.; Wonneberger, H.; Mullen, K.; Rabe, J. P.; Hla, S. W.; Koch, N. Monolayer Phases of a Dipolar Perylene Derivative on Au(111) and Surface Potential Build-Up in Multilayers. *Langmuir* **2016**, *32*, 3587−600.
(24) Pivetta, M.; Blüm, M.-C.; Patthey, F.; Schneider, W.-D. Three-Dimensional Chirality Transfer in Rubrene Multilayer Islands on Au(111). *J. Phys. Chem. B* **2009**, *113*, 4578−4581.
(25) Mairena, A.; Zoppi, L.; Seibel, J.; Tröster, A. F.; Grenader, K.; Parschau, M.; Terfort, A.; Ernst, K.-H. Heterochiral to Homochiral Transition in Pentahelicene 2D Crystallization Induced by Second-Layer Nucleation. *ACS Nano* **2017**, *11*, 865−871.
(26) Parschau, M.; Ernst, K. H. Disappearing Enantiomorphs: Single Handedness in Racemate Crystals. *Angew. Chem., Int. Ed.* **2015**, *54*, 14422−14426.
(27) Parschau, M.; Ellerbeck, U.; Ernst, K.-H. Chirality transfer by epitaxial mismatch in multi-layered homochiral molecular films. *Colloids Surf., A* **2010**, *354*, 240−245.
(28) Racemate or conglomerate double layers have opposite or the same chirality between layers, respectively.
(29) Cao, H.; De Feyter, S. Amplification of chirality in surface-confined supramolecular bilayers. *Nat. Commun.* **2018**, *9*, 3416−3416.
(30) Lee, S.; Hirsch, B. E.; Liu, Y.; Dobscha, J. R.; Burke, D. W.; Tait, S. L.; Flood, A. H. Multifunctional Tricarbazolo Triazolophane Macrocycles: One-Pot Preparation, Anion Binding, and Hierarchical Self-Organization of Multilayers. *Chem. - Eur. J.* **2016**, *22*, 560−569.
(31) Svatek, S. A.; Perdigao, L. M. A.; Stannard, A.; Wieland, M. B.; Kondratuk, D. V.; Anderson, H. L.; O'Shea, J. N.; Beton, P. H. Mechanical Stiffening of Porphyrin Nanorings through Supramolecular Columnar Stacking. *Nano Lett.* **2013**, *13*, 3391−3395.
(32) Huang, W.; Zhao, T.-Y.; Wen, M.-W.; Yang, Z.-Y.; Xu, W.; Yi, Y.-P.; Xu, L.-P.; Wang, Z.-X.; Gu, Z.-J. Adlayer Structure of Shape-Persistent Macrocycle Molecules: Fabrication and Tuning Investigated with Scanning Tunneling Microscopy. *J. Phys. Chem. C* **2014**, *118*, 6767−6772.
(33) Iritani, K.; Ikeda, M.; Yang, A.; Tahara, K.; Hirose, K.; Moore, J. S.; Tobe, Y. Hexagonal Molecular Tiling by Hexagonal Macrocycles at the Liquid/Solid Interface: Structural Effects on Packing Geometry. *Langmuir* **2017**, *33*, 12453−12462.
(34) Hirsch, B. E.; Lee, S.; Qiao, B.; Chen, C. H.; McDonald, K. P.; Tait, S. L.; Flood, A. H. Anion-induced dimerization of 5-fold symmetric cyanostars in 3D crystalline solids and 2D self-assembled crystals. *Chem. Commun.* **2014**, *50*, 9827−9830.
(35) Wieland, M. B.; Perdigao, L. M. A.; Kondratuk, D. V.; O'Shea, J. N.; Anderson, H. L.; Beton, P. H. Height dependent molecular trapping in stacked cyclic porphyrin nanorings. *Chem. Commun.* **2014**, *50*, 7332−7335.
(36) Ciesielski, A.; Cadeddu, A.; Palma, C.-A.; Gorczynski, A.; Patroniak, V.; Cecchini, M.; Samori, P. Self-templating 2D supramolecular networks: a new avenue to reach control over a bilayer formation. *Nanoscale* **2011**, *3*, 4125−4129.
(37) Blunt, M. O.; Russell, J. C.; Gimenez-Lopez, M. d. C.; Taleb, N.; Lin, X.; Schroder, M.; Champness, N. R.; Beton, P. H. Guest-induced growth of a surface-based supramolecular bilayer. *Nat. Chem.* **2011**, *3*, 74−78.
(38) Tahara, K.; Furukawa, S.; Uji-i, H.; Uchino, T.; Ichikawa, T.; Zhang, J.; Mamdouh, W.; Sonoda, M.; De Schryver, F. C.; De Feyter, S.; Tobe, Y. Two-Dimensional Porous Molecular Networks of Dehydrobenzo[12]annulene Derivatives via Alkyl Chain Interdigitation. *J. Am. Chem. Soc.* **2006**, *128*, 16613−16625.
(39) Tobe, Y.; Tahara, K.; De Feyter, S. Adaptive Building Blocks Consisting of Rigid Triangular Core and Flexible Alkoxy Chains for Self-Assembly at Liquid/Solid Interfaces. *Bull. Chem. Soc. Jpn.* **2016**, *89*, 1277−1306.
(40) Lei, S. B.; Tahara, K.; De Schryver, F. C.; Van der Auweraer, M.; Tobe, Y.; De Feyter, S. One building block, two different supramolecular surface-confined patterns: Concentration in control at the solid-liquid interface. *Angew. Chem., Int. Ed.* **2008**, *47*, 2964−2968.
(41) Tahara, K.; Yamaga, H.; Ghijsens, E.; Inukai, K.; Adisoejoso, J.; Blunt, M. O.; De Feyter, S.; Tobe, Y. Control and induction of surface-confined homochiral porous molecular networks. *Nat. Chem.* **2011**, *3*, 714−719.
(42) Fang, Y.; Ghijsens, E.; Ivasenko, O.; Cao, H.; Noguchi, A.; Mali, K. S.; Tahara, K.; Tobe, Y.; De Feyter, S. Dynamic control over supramolecular handedness by selecting chiral induction pathways at the solution−solid interface. *Nat. Chem.* **2016**, *8*, 711−717.
(43) Tahara, K.; Noguchi, A.; Nakayama, R.; Ghijsens, E.; De Feyter, S.; Tobe, Y. Reversing the Handedness of Self-Assembled Porous Molecular Networks through the Number of Identical Chiral Centres. *Angew. Chem., Int. Ed.* **2019**, *58*, 7733−7738.
(44) Balandina, T.; Tahara, K.; Sandig, N.; Blunt, M. O.; Adisoejoso, J.; Lei, S. B.; Zerbetto, F.; Tobe, Y.; De Feyter, S. Role of Substrate in Directing the Self-Assembly of Multicomponent Supramolecular Networks at the Liquid-Solid Interface. *ACS Nano* **2012**, *6*, 8381−8389.
(45) Barlow, S. M.; Raval, R. Complex organic molecules at metal surfaces: bonding, organisation and chirality. *Surf. Sci. Rep.* **2003**, *50*, 201−341.
(46) Elemans, J.; De Cat, I.; Xu, H.; De Feyter, S. Two-dimensional chirality at liquid-solid interfaces. *Chem. Soc. Rev.* **2009**, *38*, 722−736.
(47) Raval, R. Chiral expression from molecular assemblies at metal surfaces: insights from surface science techniques. *Chem. Soc. Rev.* **2009**, *38*, 707−721.
(48) Yoon, T. P.; Jacobsen, E. N. Privileged Chiral Catalysts. *Science* **2003**, *299*, 1691−1693.
(49) All of the data shown in the main text are done in a liquid cell using 40 μL of solution. Similar results can be obtained by the simple drop-casting method using 4 μL of solution (for more detail see the Supporting Information). Large quantity of solution are used to minimize the concentration change due to evaporation.

https://dx.doi.org/10.1021/jacs.0c00108
J. Am. Chem. Soc. 2020, 142, 8662−8671

(50) Crivillers, N.; Furukawa, S.; Minoia, A.; Ver Heyen, A.; Mas-Torrent, M.; Sporer, C.; Linares, M.; Volodin, A.; Van Haesendonck, C.; Van der Auweraer, M.; Lazzaroni, R.; De Feyter, S.; Veciana, J.; Rovira, C. Two-Leg Molecular Ladders Formed by Hierarchical Self-Assembly of an Organic Radical. *J. Am. Chem. Soc.* **2009**, *131*, 6246−6252.
(51) Plass, K. E.; Grzesiak, A. L.; Matzger, A. J. Molecular packing and symmetry of two-dimensional crystals. *Acc. Chem. Res.* **2007**, *40*, 287−293.
(52) Hisaki, I.; Senga, H.; Sakamoto, Y.; Tsuzuki, S.; Tohnai, N.; Miyata, M. Specific Interaction between Chloroform and the Pockets of Triangular Annulene Derivatives Providing Symmetry Carry-Over Crystallization. *Chem. - Eur. J.* **2009**, *15*, 13336−13340.
(53) Hisaki, I.; Sakamoto, Y.; Shigemitsu, H.; Tohnai, N.; Miyata, M.; Seki, S.; Saeki, A.; Tagawa, S. Superstructure-dependent optical and electrical properties of an unusual face-to-face, π-stacked, one-dimensional assembly of dehydrobenzo[12]annulene in the crystalline state. *Chem. - Eur. J.* **2008**, *14*, 4178−4187.

https://dx.doi.org/10.1021/jacs.0c00108
J. Am. Chem. Soc. 2020, 142, 8662−8671